Separation Science and Technology
Publication details, including instructions for authors and subscription information:
http://www.informaworld.com/smpp/title~content=t713708471

Effects of Proton-Exchange Membrane Fuel-Cell Operating Conditions On Charge Transfer Resistances Measured by Electrochemical Impedance Spectroscopy

D. Aaron[a]; S. Yiacoumi[a]; C. Tsouris[ab]
[a] School of Civil and Environmental Engineering, Georgia Institute of Technology, Atlanta, Georgia, USA [b] Oak Ridge National Laboratory, Oak Ridge, Tennessee, USA

To cite this Article Aaron, D. , Yiacoumi, S. and Tsouris, C.(2008) 'Effects of Proton-Exchange Membrane Fuel-Cell Operating Conditions On Charge Transfer Resistances Measured by Electrochemical Impedance Spectroscopy', Separation Science and Technology, 43: 9, 2307 — 2320
To link to this Article: DOI: 10.1080/01496390802148613
URL: http://dx.doi.org/10.1080/01496390802148613

Separation Science and Technology, 43: 2307–2320, 2008

ISSN: 0149-6395 print/1520-5754 online
DOI: 10.1080/01496390802148613

Taylor & Francis
Taylor & Francis Group

Effects of Proton-Exchange Membrane Fuel-Cell Operating Conditions On Charge Transfer Resistances Measured by Electrochemical Impedance Spectroscopy

D. Aaron,[1] S. Yiacoumi,[1] and C. Tsouris[1,2]
[1]School of Civil and Environmental Engineering, Georgia Institute of Technology, Atlanta, Georgia, USA
[2]Oak Ridge National Laboratory, Oak Ridge, Tennessee, USA

Abstract: Proton-exchange-membrane fuel cells (PEMFC) are highly dependent on operating conditions, such as humidity and temperature. This study employs electrochemical impedance spectroscopy (EIS) to measure the effects of operating parameters on internal proton and electron transport resistance mechanisms in the PEMFC. Current-density experiments have been performed to measure the power production in a 25 cm^2 Nafion 117 PEMFC at varying operating conditions. These experiments have shown that low humidity and low temperature contribute to decreased power production. EIS is currently employed to provide a better understanding of the mechanisms involved in power production by calculating the specific resistances at various regions in the PEMFC. Experiments are performed at temperatures ranging from 30 to 50°C, feed humidities from 20 to 98%, and air stoichiometric ratios from 1.33 to 2.67. In all experiments, the hydrogen feed stoichiometric ratio was approximately 4.0. EIS is used to identify which transport steps limit the power production of the PEMFC over these ranges of conditions. The experimental data are analyzed via comparison to equivalent circuit models (ECMs), a technique that uses an electrical circuit to represent the electrochemical and transport properties of the PEMFC. These studies will aid in designing fuel cells that are more tolerant to wide-ranging operating conditions. In addition, optimal operating conditions for PEMFC operation can be identified.

Keywords: PEM fuel cell, electrochemical impedance spectroscopy, internal resistance

Received 25 October 2007; accepted 2 April 2008.
Address correspondence to C. Tsouris, Oak Ridge National Laboratory, Oak Ridge, Tennessee 37831-6181, USA. E-mail: tsourisc@ornl.gov

INTRODUCTION

Fuel cells have become a widely studied energy conversion technology due to their high efficiency, simplicity in terms of moving parts, and wide-ranging array of configurations, fuels, and applications. Low-temperature, proton-exchange membrane fuel cells (PEMFCs) are of special interest for automobiles and other portable energy applications. A primary drawback, however, is cost, especially in the form of expensive precious-metal catalysts. Because of the high cost, optimal catalyst utilization and transport conditions are desired to increase the power output per unit cost.

The fuel cell can be readily divided into three distinct regions, each with its own interfaces, transport processes, and electrochemical reactions that should be understood and optimized. As hydrogen is introduced into the fuel cell, the first region is the anode. Outside of the catalyst layer, transport occurs by bulk fluid flow in the flow channels and gas diffusion layer (GDL). In the catalyst layer, hydrogen adsorbs onto a catalyst (Pt in most low-temperature cases) and the resultant protons must follow a continuous channel of water from the catalyst to the membrane to continue through the PEMFC. In this three-phase region (gaseous water and hydrogen, solid catalyst, and liquid water), transport is not well-understood and the catalyst utilization efficiency is affected by humidity and temperature. Many interfaces are important in this region: membrane-catalyst-gas, membrane-support-gas, membrane-gas, and catalyst-gas (see Fig. 1). Transport may occur across all of these interfaces, but possibly the most important interface is the membrane-catalyst-gas. This is the interface where catalyst efficiency is determined, a major cost factor for fuel cells. After hydrogen dissociates into protons and electrons in the anode catalyst layer, the protons must diffuse to, and then through, the proton-exchange membrane (PEM). While there are no chemical reactions for protons occurring in the PEM, resistances to ionic transport are present and can contribute to cell power loss. After protons

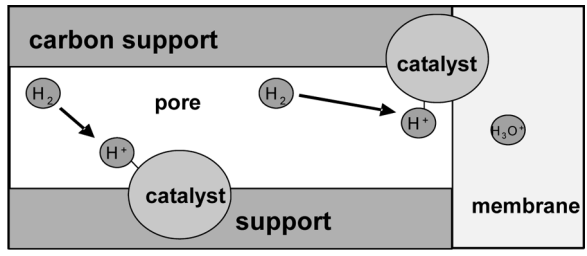

Figure 1. Conceptual summary of interfaces in the anode catalyst layer (1).

diffuse through the PEM, they come to the cathode catalyst layer. It is in this region that protons and electrons (from the feed hydrogen) combine with oxygen to form water. This water can then diffuse back through the membrane or evaporate and exhaust from the system.

Two very important parameters in each of the three regions are water content and temperature. Temperature is controlled externally while water content is controlled by feed humidity and electrical current. Temperature affects catalytic reaction rates and transport of protons through the PEM (2,3). Water is the medium for proton transport in a PEMFC, thus there must be a continuous path of water from the anode catalyst to the cathode catalyst. Too little water in the anode catalyst layer may result in no path for protons to enter the PEM; too much water can cover the catalyst, making hydrogen contact with catalyst difficult. In the PEM, there must be enough water to form pathways connecting the two electrode catalyst layers.

Electrochemical impedance spectroscopy has been utilized to characterize internal resistance mechanisms that limit fuel cell power production. Prior work has addressed the effects of catalyst layer support on internal resistance (4,5). Important among these mechanisms are charge transfer resistance, electrical double layer capacitance, and diffusion resistances. Resistances to transport can be thought of in terms of an electrical circuit, where flow is inhibited by impedances. The definition of impedance, as used in EIS, is given by Equation 1:

$$Z = \frac{V_o \sin(\omega t)}{I_o \sin(\omega t + \phi)} = Z_o \frac{\sin(\omega t)}{\sin(\omega t + \phi)} \tag{1}$$

Current (I_o) and ϕ (phase shift) can be measured as a function of an applied AC signal (V_o), allowing the determination of impedance, Z (6). By applying this signal over a spectrum of frequency, the magnitudes of various resistances and capacitances can be determined via an equivalent circuit model (7). It is expected that temperature and water content will affect these impedances, just as they affect cell power production. Current density has been previously shown to greatly affect EIS results (8,9), thus cell temperature, feed humidity, and feed flow rates are of interest. This paper will present results from exploring the effects of temperature, air-side humidity, and air flow rate on charge transfer resistances in the PEMFC.

EXPERIMENTAL

A 25 cm^2 active area PEMFC was utilized in these studies. This fuel cell has gold-plated aluminum endplates, graphite current collectors with

four-channel serpentine feed distributors, and a membrane-electrode assembly (MEA) with carbon/platinum catalyst layers and a Nafion 117 PEM (made by Asia Pacific Fuel Cells, Taiwan). The MEA was also made by Asia Pacific Fuel Cells, via hot pressing the layers together. A test stand with temperature, feed pressure, feed humidification, and feed flow rate controls was used. EIS data were generated and taken by a Gamry Instruments series 750 G Galvanostat/potentiostat/zero-resistance ammeter. Equivalent circuit models (ECMs) were constructed and tested using Gamry EChem Analyst software. This package utilizes a least-squares optimization routine to determine impedances in an ECM. The ECM that was used in these studies is shown in Fig. 2, as described in previous work performed by Page et al. (10). Various ECMs have been proposed, but the ECM employed here is very common in the literature. Other ECMs include a model with a resistor in series with a parallel resistor-capacitor component (7,10) and various models that expand the electrodes to include other circuit elements to describe diffusion resistances. These alternative models were tested and found to not offer significantly better fits to the experimental results. Ultimately, it is desirable to use the simplest ECM that physically describes the system. From the anode side to the cathode, there is a high frequency resistance, a parallel component with a charge transfer resistance and electrical double layer capacitance, a resistor for the PEM, and another parallel component similar to the anode to represent the cathode electrode.

To maintain a linear response between the applied AC potential and current (see Equation 1), a 10 mV signal was applied to the fuel cell at all frequencies. The frequency range was from 100 mHz to 100 kHz with 10

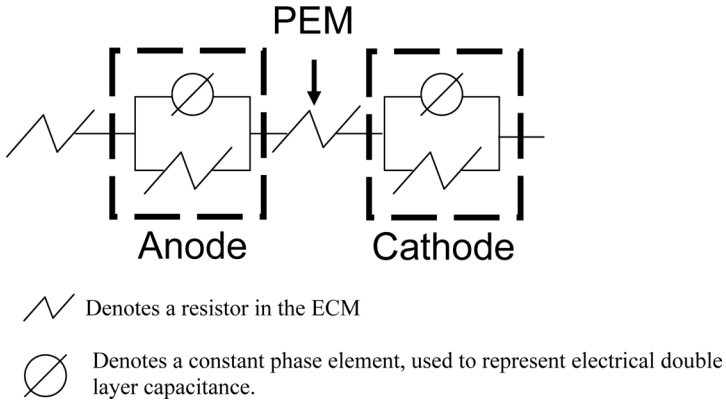

Figure 2. ECM with two electrodes, PEM, and external, high-frequency resistance.

measurements per decade. Each 10 decade scan required approximately 2.5 minutes; cell voltage was monitored during scans to verify that no noticeable drift was occurring. This determination was qualitative since the cell output potential was slightly affected by the signal, most noticeably at low frequencies.

The goal of these experiments was to measure the effects of operational parameters on internal charge transfer resistances. The effects of cell temperature, air feed humidity, and air feed flow rate were investigated. The matrix of conditions for experiments is shown in Table 1. As a summary, the control conditions were 50°C, 98% humidity for both feeds, 20 sccm hydrogen and 45.1 sccm air feed. As one operating parameter was adjusted, the others were maintained at the control conditions. In addition to these experiments, the transient response of the fuel cell to a stepwise increase in air-side humidity from 0% to 98% RH was measured by EIS. In this experiment, the cell was allowed to operate with 0% air-side RH for approximately 30 minutes. Then the air-side humidity was quickly increased to 98% and EIS performed during the response period until steady state was achieved. Since the change in cell voltage was slow over time (1 mV/min) during this response, fast EIS measurements could be completed without significant changes in the performance of the fuel cell. Also, the cell was allowed to run for approximately 30 minutes before performing EIS, as there is a quick startup period and then a slow increase in power over time until steady power output is achieved.

In all the experiments performed, the hydrogen flow rate was maintained between 19.9 and 20.3 sccm; this flow rate corresponds to a stoichiometric ratio of approximately 4.3 since the cell consumes approximately 4.7 sccm of hydrogen. It should be mentioned here that the stoichiometric ratio is defined as the ratio of reactant flow rate fed to the

Table 1. Matrix of experiments exploring temperature, air humidity, and air flow rate

Temperature (°C)	Air humidity (%RH)	Air flow (sccm)
31	98	45
40	98	45
51	98	45
51	98	45
51	20	45
51	63	45
50	98	20
50	98	30

minimum flow rate for stable operation. A hydrogen feed of 20 sccm was chosen to correspond to a 1:1 ratio with the minimum air flow rate for cell operation. Below 20 sccm air flow, the cell was unsteady; below 15 sccm air flow, the cell did not produce power. Also, the humidification columns were maintained at a temperature 10°C warmer than the cell temperature. Both air and hydrogen feed channels were open to the atmosphere at the outlet, so no back pressure was applied to either side. The load in all experiments was set at 5 Ω and resulted in current density ranging from 34–50 W/m^2.

Each effect (temperature, humidity, air flow rate, and transient humidity response) was investigated after completely drying out and cooling the fuel cell. The same startup procedure was followed for each series of experiments, except for the transient humidity response. For temperature, humidity, and air flow rate, the feed gas humidifiers were heated to 10°C above the desired fuel cell temperature. Once the humidifiers were thermally stable, the feed gases were turned on to stoichiometric ratios of approximately 4.0. When the feed gases began passing through the cell, the cell was heated to the experimental temperature. The high feed rate of air was maintained for approximately 30 minutes to hydrate the MEA. After this 30 minute period, the air feed rate was set to the experimental rate and the cell allowed to equilibrate. The hydrogen feed rate was maintained at a stoichiometric ratio of 4.0. The cell was then left at the experimental conditions for approximately one hour for stabilization; steady state was confirmed by monitoring the output voltage. Once the output voltage was stable (varying by no more than 1 mV/min), EIS was performed.

No experiments changing the condition of the hydrogen feed were conducted because it was found that the cell was unsteady at low hydrogen humidity and low feed rate. Thus, variations in the air feed were explored as they allowed steady cell operation, yet still had appreciable effects on charge transfer resistances throughout the PEMFC. Experiments to qualitatively explore the effects of combined air flow rate and humidity changes were performed, but are not included in this paper.

RESULTS

Temperature Effects

As the cell temperature increased, an increase in cell power output was observed. At the same time, charge transfer resistances in the anode, PEM, and cathode all decreased. The anode and cathode resistances both decreased by approximately 10% while the PEM resistance

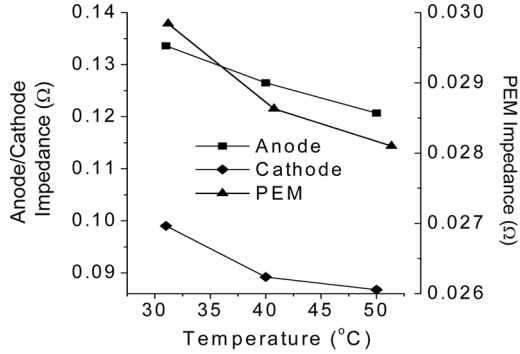

Figure 3. Anode, PEM, and cathode charge transfer resistances as a function of temperature. Hydrogen flow: 20.1 sccm (98% RH), air flow: 45.1 sccm; 98% RH for both feed streams.

decreased by approximately 5% over the range of temperature studied. The greater decrease in the electrodes (compared to the PEM) is believed to be due to faster reactions at higher temperature, e.g., higher collision rate of reactant molecules with the catalyst (see Fig. 1). The impedance results are shown in Fig. 3. Figure 4 is the Nyquist plot of the impedance data. The Nyquist plot is useful for identifying resistances in the cell at both the high frequency (to the left of the curve) and low frequency (to the right of the curve) intercepts on the Z_{Real} axis. These resistances

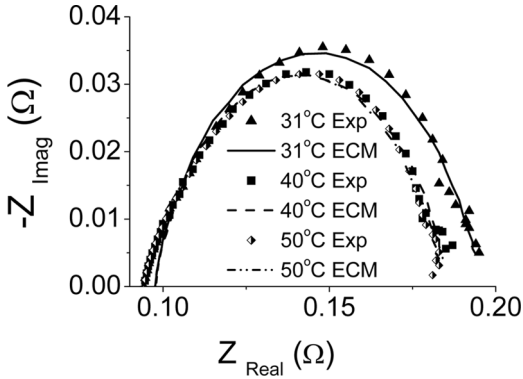

Figure 4. Nyquist plot for the PEMFC at 31, 40, and 50°C showing the imaginary impedance as a function of real impedance. Frequency increases from right to left on the curve. Hydrogen flow: 20.1 sccm (98% RH), air flow: 45.1 sccm; 98% RH for both feed streams.

are helpful for obtaining initial guesses used in the ECM optimization. Since the Nyquist plot contains no real frequency data, it was only used to provide the initial guesses for the ECM fit optimization.

On the Nyquist plot, the imaginary component ($-Z_{Imag}$) is a result of the phase shift while the real component (Z_{Real}) is based on the magnitude of impedance measured in EIS. In this case, charge transfer resistances, in which protons are transferred from the electrode to the electrolyte, decreased with increasing power production. This is reasonable, since decreasing transport resistances in the fuel cell should allow greater throughput of protons and electrons. Indeed, a good first indicator of decreased charge transfer resistances is increased power production. It should be noted that the anode provided the greatest resistance over the whole temperature range studied. The anode resistance was consistently approximately 35 mΩ greater than the cathode resistance and 100 mΩ greater than the PEM resistance.

Effects of Air-side Humidity

Presented in Fig. 5 are the responses of anode, PEM, and cathode charge transfer resistances to air-side humidity. Experiments in which the hydrogen feed humidity was varied over a large range could not be carried out because the cell either did not produce power or was too unstable for EIS

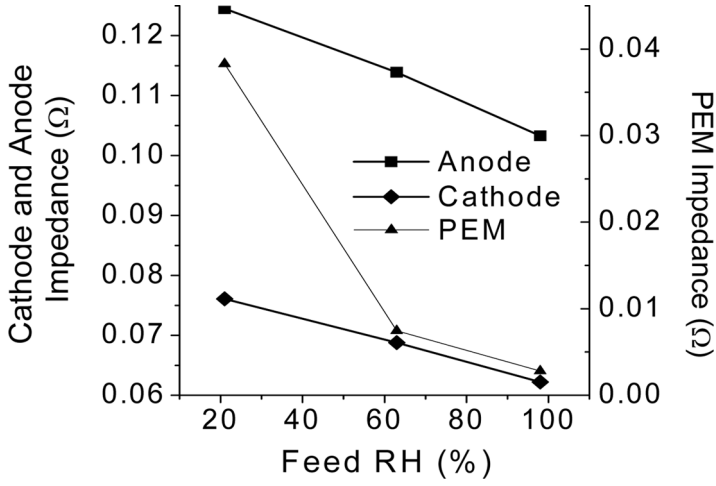

Figure 5. Anode, PEM, and cathode charge transfer resistances as a function of air-side humidity. Hydrogen flow: 20.0 sccm (98% RH), air flow: 45.1 sccm; cell temperature was maintained at 51°C.

analysis at low humidification. Thus, experiments were performed where hydrogen humidification was held constant at 98%. It can be seen in Fig. 5 that resistances in all three regions decreased as humidity increased, especially in the PEM. At the same time, the cell power output increased. All of the experiments were performed at 50°C because the cooler temperatures eventually resulted in suspected flooding of flow channels in the anode, as indicated by short disruptions in power output.

Figures 6 and 7 show the Bode and Nyquist plots, respectively, of the data collected in these air-side humidity experiments. It can be seen in Fig. 6 that very slight oscillations in phase shift and impedance occur in the low frequency region. While these can be the signature of flooding conditions, it is not believed that flooding occurred because the cell power output did not drop or oscillate, as would be expected with a flooding event (11). Flooding occurs in a PEMFC when liquid water builds up in the catalyst layer, GDL, or flow channels and blocks the flow of gas. Also, flooding is expected to cause much larger oscillations in power output, impedance, and phase shift due to unstable performance. At low signal frequency, oscillations in cell potential were observed with a multimeter, but these oscillations were a result of the EIS signal passing through the cell, as determined by comparing the signal generation and multimeter reading. It is difficult, when looking at Fig. 6, to see a large change in impedance between the various air-side humidification levels. Above 5 Hz, there is significant overlap between the three different series of impedances. However, when analyzing the data via the ECM, it is observed that all of the charge transfer resistances decrease, and power measurements indicate increased power production at greater

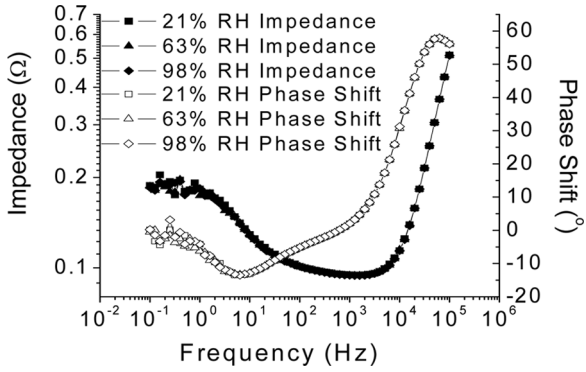

Figure 6. Bode plot showing impedance and phase shift for the PEMFC at multiple air-side humidity settings. Hydrogen flow: 20.2 sccm (98% RH), air flow: 45.1 sccm; cell temperature was held constant at 50°C.

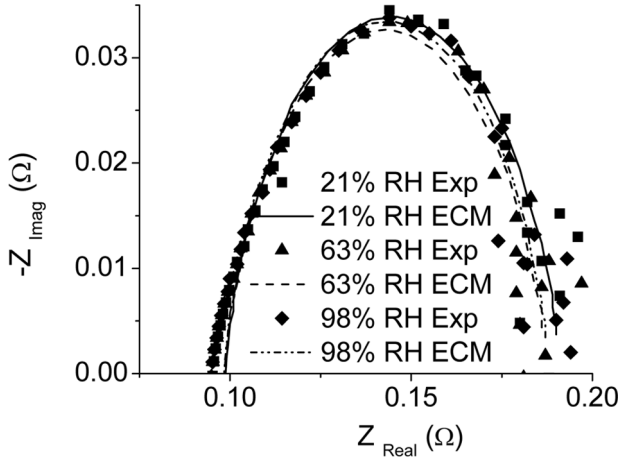

Figure 7. Nyquist plot for the PEMFC at multiple air-side humidity settings. Hydrogen flow: 20.2 sccm (98% RH), air flow: 45.1 sccm; cell temperature was held constant at 50°C.

humidification. The Nyquist plot in Fig. 7 supports this result, as seen where the low frequency data show a decrease of the summed resistances. While there is scatter in the data, the increase in power production with increased humidity supports the model results showing decreased resistance at higher air-side humidity.

Effects of Air Flow Rate

The effect of air flow rate on the three resistances was also explored; these results are illustrated in Fig. 8. All three resistances decreased slightly: 3.3% for the anode and approximately 6% for both the PEM and cathode. Since the air flow rate was adjusted on the cathode side, it is reasonable for the cathode side to be affected more than the anode. Similar to the results from the temperature experiments, the anode has the greatest impedance: approximately 35 mΩ greater than the cathode and 90 mΩ greater than the PEM. It can be seen that the air flow rate had little effect on the transport resistances in the fuel cell, as long as it was greater than the minimum flow rate for cell operation (which was found to be approximately 15 sccm). Additionally, the cell power output changed very little between the three air flow rates, from 40.0 W/m^2 at 20 sccm to 41.0 W/m^2 at 40 sccm. However, even though the air flow rate had little effect on the charge transfer resistances and power output, it is still

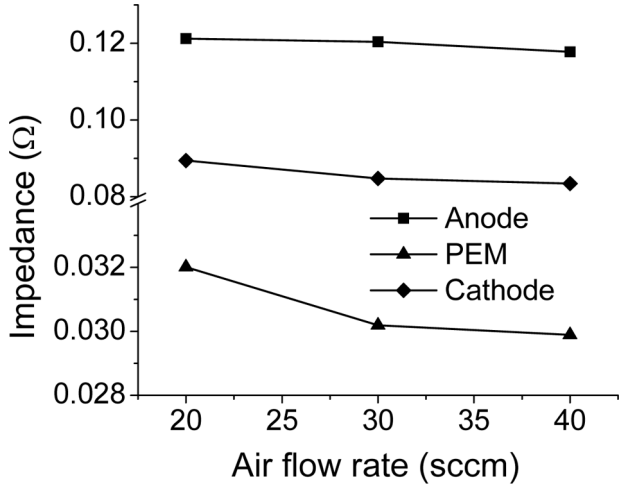

Figure 8. Anode, PEM, and cathode charge transfer resistances as a function of air flow rate. Hydrogen flow rate was held at 20 sccm (stoichiometric ratio of ~4.3); cell temperature was constant at 50°C and both feed streams were at 98% RH.

vital to maintain air flow above a stoichiometric air ratio of one or the cell ceases operation very quickly.

Transient Response to an Increase in Air-side Humidity

Finally, a transient response of the fuel cell impedances to a step-wise increase in air humidity was measured at a cell temperature of 51°C. These results can be seen in Fig. 9. Counter to what was expected, both the anode and cathode charge transfer resistances increased over time; the cell power output steadily increased over this entire time period. Thus, despite the increases in charge transfer resistance for these two regions, the overall cell power increased over time. Upon further review of the data, it was found that the electrical double layer capacitance impedances decreased over time; thus, the overall impedance decreased, but this is not seen when only considering the charge transfer resistances. Even though the two charge transfer resistances did not become steady over time, the power output of the fuel cell became steady within 20 minutes of applying air-side humidification. At this point, the experiment was terminated. EIS experiments measuring the transient response of the cell to a reduction in air-side humidity were not performed, though may be of interest in the future.

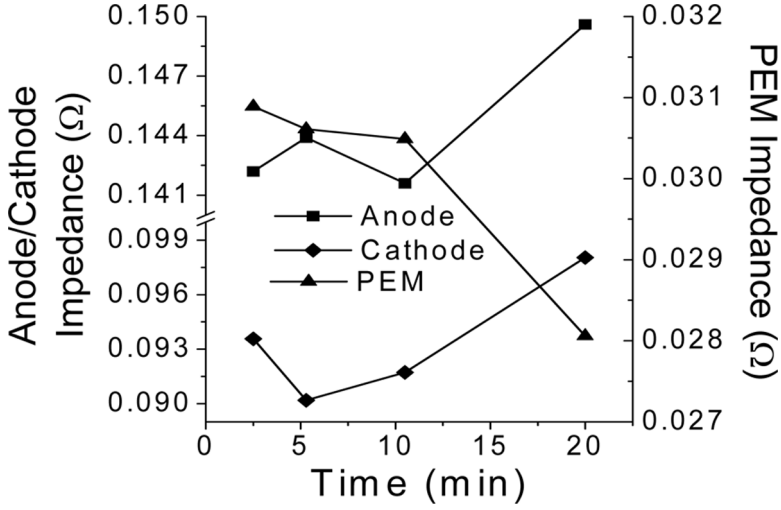

Figure 9. Response of anode, PEM, and cathode charge transfer resistances as a function of time after stepping air-side humidity from 0% to 98% RH. Hydrogen flow: 19.9 sccm (98% RH), air flow: 45.1 sccm; cell temperature was 51°C.

It was also observed in these experiments that impedance is not a state function based on operating conditions of the steady-state PEMFC. A repeat of the transient response showed the same trend for charge transfer resistance, but values were approximately 8% greater than in the first experiment. Experiments to establish a reliable standard deviation were not performed; however, the model results fit well the experimental data so that the differences in impedance are not believed to be due to poor model fit. It is believed that the startup of the fuel cell affects impedance values, possibly because some conformational changes that occur during startup persist after steady state is achieved. For example, the distribution of water channels linking the anode-PEM interface may form uniquely during each startup. In addition to the impedances behaving this way, the cell power output is not always constant from one experiment to another; each startup resulted in different cell potential (and, consequently, power production) at steady state, on the order of 10 mV out of 750 mV.

CONCLUSION

EIS was used to study the effects of cell temperature, air feed humidity, air feed rate, and transient response to a step-wise change in air feed

humidity. Anode charge transfer resistance, PEM ionic resistance, and cathode charge transfer resistance all decreased as temperature increased; there was also a corresponding increase in power production. The three resistances also decreased drastically as air feed humidity increased (this is not the case for the transient response, however), which also resulted in increased power production. The air flow rate did not have a large effect on the three charge transfer resistances. In all of the experiments, the greatest resistance was identified in the anode; this resistance was consistently 30–90 mΩ greater than in the cathode and PEM, respectively.

The air-side humidity had the greatest effect on charge transfer resistances in these experiments. Operating temperature also had a significant effect, while the air-side flow rate had relatively little effect, as long as it was maintained at least at a stoichiometric ratio of approximately 1.2. Humidification of both the air and hydrogen feeds and high temperature (below that leading to the degradation of the PEM) are important for optimal power production. Further experiments should focus on investigating resistances at greater temperatures. Greater reactant feed rate is also of interest to explore a wider range of flow rates.

The transient response to a step-wise air humidity increase illustrates an important consideration when performing EIS: charge transfer resistances do not always decrease as power production increases. Even though these resistances increased in both electrodes over time, the power production increased. Charge transfer resistances are often a good indicator of the overall internal impedance, but do not always provide adequate information about the performance of a fuel cell. Thus, it is always beneficial to consider power output observations, as well as all ECM impedances, when performing EIS analysis of a PEMFC.

ACKNOWLEDGMENT

This work is a collaboration between the University of Tennessee, Georgia Institute of Technology, and Oak Ridge National Laboratory and is supported by the U.S. Department of Energy, Office of Basic Energy Sciences, through the grant DE-FG02-05ER15723 to the University of Tennessee.

NOMENCLATURE

ECM:	equivalent circuit model
EIS:	electrochemical impedance spectroscopy
PEMFC:	proton-exchange membrane fuel cell (also polymer electrolyte membrane fuel cell)

REFERENCES

1. Liu, J.; Esai Selvan, M.; Cui, S.; Edwards, B.J.; Keffer, D.J.; Steele, W.V. (2008) Molecular-level modeling of the structure and wetting of electrode/electrolyte interfaces in hydrogen fuel cells. *J. Phys. Chem. C*, *112* (6): 1985–1993.
2. Andreaus, B.; McEvoy, A.; Scherer, G. (2002) Analysis of performance losses in polymer electrolyte fuel cells at high current densities by impedance spectroscopy. *Electrochimica Acta*, *4*: 2223–2229.
3. Cui, S.T.; Liu, J.; Esai Selvan, M.; Keffer, D.J.; Edwards, B.J.; Steele, W.V. (2002) A molecular dynamics study of a Nafion polyelectrolyte membrane and the aqueous phase structure for proton transport. *J. Phys. Chem. B*, *111* (13): 3469–3475.
4. Springer, T.E.; Zawodzinski, T.A.; Wilson, M.S.; Gottesfeld, S. (1996) Characterization of polymer electrolyte fuel cells using AC impedance spectroscopy. *J. Electrochem. Soc.*, *143* (2): 587–599.
5. Gerteisen, D.; Hakenjos, A.; Schumacher, J.O. (2007) AC impedance modelling study on porous electrodes of proton exchange membrane fuel cells using an agglomerate model. *Journal of Power Sources*, *173* (1): 346–356.
6. Gamry Instruments. Basics of Electrochemical Impedance Spectroscopy. Application Note, www.gamry.com/App_Notes/Index.htm. 2006.
7. Gomadam, P.; Weidener, J. (2005) Analysis of electrochemical impedance spectroscopy in proton exchange membrane fuel cells. *Int. J. Energy Res.*, *29*: 1133–1151.
8. Wiezell, K.; Gode, P.; Lindbergh, G. (2006) Steady-state and EIS investigations of hydrogen electrodes and membranes in polymer electrolyte fuel cells: I. Modeling. *Journal of the Electrochemical Society*, *153* (4): A749–A758.
9. Wiezell, K.; Gode, P.; Lindbergh, G. (2006) Steady-state and EIS investigations of hydrogen electrodes and membranes in polymer electrolyte fuel cells: II. Experimental. *Journal of the Electrochemical Society*, *153* (4): A759–A764.
10. Page, S.; Anbuky, A.; Krumdieck, S.; Brouwer, J. (2007) Test method and equivalent circuit modeling of a PEM fuel cell in a passive state. *Energy Conversion, IEEE Transaction on*, *22* (3): 764–773.
11. Le Canut, J.; Abouatallah, R.; Harrington, D. (2006) Detection of membrane drying, fuel cell flooding, and anode catalyst poisoning on PEMFC stacks by electrochemical impedance spectroscopy. *J. Electrochem. Soc.*, *153* (5): A857–A864.